the substrate (*16*). However, the statistics for more than 40 spherical quantum dots in our measurement at room temperature shows that the average polarization factor is <10%. Because we used an objective lens with a large numerical aperture (e.g., 1.4) that depolarizes light, the limit for polarization factor that our experimental setup can obtain is ~80%. Thus, the emission from quantum rods with an aspect ratio greater than 2:1 is essentially purely linearly polarized, which is consistent with theoretical results.

To further test the calculations, we measured the global Stokes shift of the quantum rods experimentally. For rods with a fixed width, we found that the global Stokes shift decreased slightly from spherical dots to short rods and then increased with length to more than 100 meV, which is much greater than that of spherical quantum dots with the same diameter (Fig. 2B). This response qualitatively agrees with the theoretical results. A dielectric model was previously proposed to explain the anisotropic polarization of the emission from porous silicon, assuming that porous silicon is an aggregate of Si nanocrystals with different shapes (*28*). Concentration of the field lines in the region of high dielectric constant may contribute to the polarization of the emission from CdSe quantum rods as well (Fig. 4C). However, the nonmonotonic behavior of the Stokes shift versus the aspect ratio shows that the level crossing is the dominant factor at a small aspect ratio. A larger Stokes shift means a smaller overlap area between absorption and emission spectra, which is desirable in applications such as light-emitting diodes, where reabsorption reduces the total efficiency. We also see some discrepancies between the theory and experiments, however. The turning point from the experiments does not coincide with that from the theoretical calculations, and the experimental Stokes shift values are always greater than the theoretical ones. This difference could be due to factors such as the electric field caused by the dipole moment (*29, 30*) and the electron-phonon coupling (*31, 32*), which are not considered in the calculations.

The emission polarization of CdSe nanocrystals can be greatly modified by slightly changing their shapes without much of an increase in the complication of the preparation. This change greatly improves their potential in applications. The compression of emission to a single polarization axis makes these nanocrystals ideal for many orientation-sensitive applications. As emitters in lasers, CdSe quantum rods should increase power efficiency and lower the pumping threshold. They can also be used as labels in biological systems to study conformational change and energy transfer. Furthermore, the anisotropic geometry of longer quantum rods makes it possible to align them on a flat surface over a large area and therefore makes it feasible to use them in polarized light–emitting diodes and flat panel displays.

References and Notes

1. A. P. Alivisatos, *Science* **271**, 933 (1996).
2. L. E. Brus, *Appl. Phys. A* **53**, 465 (1991).
3. A. P. Alivisatos, *J. Phys. Chem.* **100**, 13226 (1996).
4. M. A. Hines, P. Guyot-Sionnest, *J. Phys. Chem.* **100**, 468 (1996).
5. X. G. Peng *et al.*, *J. Am. Chem. Soc.* **119**, 7019 (1997).
6. R. Leon, P. M. Petroff, D. Leonard, S. Fafard, *Science* **267**, 1966 (1995).
7. J. Heydenreich *et al.*, *Phys. Rev. Lett.* **74**, 4043 (1995).
8. M. Danek *et al.*, *J. Cryst. Growth* **145**, 714 (1994).
9. C. B. Murray, C. R. Kagan, M. G. Bawendi, *Science* **270**, 1335 (1995).
10. M. Bruchez Jr., M. Moronne, P. Gin, S. Weiss, A. P. Alivisatos, *Science* **281**, 2013 (1998).
11. W. C. W. Chan, S. Nie, *Science* **281**, 2016 (1998).
12. V. Colvin, M. Schlamp, A. P. Alivisatos, *Nature* **370**, 354 (1994).
13. B. O. Dabbousi, M. G. Bawendi, O. Onotsuka, M. F. Rubner, *Appl. Phys. Lett.* **66**, 1316 (1995).
14. V. I. Klimov *et al.*, *Science* **290**, 314 (2000).
15. Al. Efros, *Phys. Rev. B* **46**, 7448 (1992).
16. S. A. Empedocles, R. Neuhauser, M. G. Bawendi, *Nature* **399**, 126 (1999).
17. X. Peng *et al.*, *Nature* **404**, 59 (2000).
18. C. B. Murray, D. J. Norris, M. G. Bawendi, *J. Am. Chem. Soc.* **115**, 8706 (1993).
19. X. G. Peng, J. Wickham, A. P. Alivisatos, *J. Am. Chem. Soc.* **120**, 5343 (1998).
20. L. Manna, E. C. Scher, A. P. Alivisatos, *J. Am. Chem. Soc.* **122**, 12700 (2000).
21. Al. Efros *et al.*, *Phys. Rev. B* **54**, 4843 (1996).
22. Al. Efros, M. Rosen, *Annu. Rev. Mater. Sci.* **30**, 475 (2000).
23. L.-W. Wang, A. Zunger, *Phys. Rev. B* **53**, 9579 (1996).
24. W. Yang *et al.*, unpublished results.
25. Z. A. Peng, X. G. Peng, *J. Am. Chem. Soc.* **123**, 1389 (2001).
26. T. Ha, T. A. Laurence, D. S. Chemla, S. Weiss, *J. Phys. Chem. B* **103**, 6839 (1999).
27. This scheme overcomes the intensity fluctuation of the luminescence from a single nanocrystal due to "blinking" and bleaching [M. Mirmal *et al.*, *Nature* **383**, 802 (1996)] and therefore can be used in room temperature measurements.
28. D. Kovalev *et al.*, *Appl. Phys. Lett.* **67**, 1585 (1995).
29. E. Rabani *et al.*, *J. Chem. Phys.* **110**, 5355 (1999).
30. M. Shim, P. Guyot-Sionnest, *J. Chem. Phys.* **111**, 6955 (1999).
31. M. C. Klein, F. Hache, D. Ricard, C. Flytzanis, *Phys. Rev. B* **42**, 11123 (1990).
32. A. P. Alivisatos *et al.*, *J. Chem. Phys.* **90**, 3463 (1989).
33. Supplemental Web material is available on *Science* Online at www.sciencemag.org/cgi/content/full/1060810/DC1.

34. We thank X. Peng for inspiring discussion and R. Zalpuri and G. Vrdoljak at the Electron Microscope Lab at the University of California, Berkeley, for assistance in TEM measurement. This work is supported by the Director, Office of Energy Research, Office of Science, and Division of Materials Sciences of the U.S. Department of Energy (DOE) under contract DE-AC03-76SF00098, by the NIH National Center for Research Resources (grant 1 R01 RR-14891-01) under the same DOE contract number, and by the Department of Defense Advanced Research Projects Agency under grant ONR N00014-99-1-0728. L.W. is supported by the Director, Office of Science, Division of Mathematical, Information, and Computational Science of DOE under contract DE-AC03-76SF00098. This research used resources of the National Energy Research Scientific Computing Center, which is supported by the Office of Science of DOE.

19 March 2001; accepted 18 April 2001
Published online 3 May 2001;
10.1126/science.1060810
Include this information when citing this paper.

Chiral Sign Induction by Vortices During the Formation of Mesophases in Stirred Solutions

Josep M. Ribó,[1]* Joaquim Crusats,[1] Francesc Sagués,[2] Josep Claret,[2] Raimon Rubires[1]

Achiral diprotonated porphyrins, forming homoassociates in aqueous solution, lead to spontaneous chiral symmetry breaking. The unexpected result is that the chirality sign of these homoassociates can be selected by vortex motion during the aggregation process. This result is confirmed by means of circular dichroism spectra. These experimental findings are rationalized in terms of the asymmetric influence of macroscopic forces on bifurcation scenarios and by considering the specific binding characteristics of the porphyrin units to form the homoassociates.

When thinking about chirality induction in physicochemical processes, one has to distinguish between two completely different scenarios. In the first one, typical of an organic chemistry context and commonly described according to the standard reaction coordinate picture, asymmetric induction arises from a polarization effect acting on the reaction path (*1*). The second situation corresponds to a spontaneous symmetry breaking scenario, according to which an excess of one of the enantiomers is always obtained, although with an unpredictable sign. By invoking generic principles of nonequilibrium phenomena, this last behavior is readily interpreted with the notion of bifurcation of an unstable

[1]Department of Organic Chemistry, [2]Department of Physical Chemistry, University of Barcelona, Martí i Franquès 1, 08028-Barcelona, Catalonia, Spain.

*To whom correspondence should be addressed. E-mail: jmr@qo.ub.es

solution, which in this case corresponds to a branch of undefined chirality (*2, 3*).

Within this second scenario, signatures of chiral symmetry breaking have been mostly reported in a crystallization context (*4*). In this case, stirring can lead to an enantiomeric excess, but there is no chirality sign selection, because the actual handedness of crystals produced in a single experiment is unpredictable (*4–7*). Apart from the context of crystallization, the spontaneous appearance of chirality, although also without sign induction, had been reported previously in aggregation processes of both thermotropic and lyotropic liquid crystals (*8–10*). Strikingly different from these observations, we report statistically robust experimental evidence that a macroscopic chiral factor (vortex motion) selects the chirality of a supramolecular structure, which is detected at the molecular level. Our observations are interpreted in terms of hydrodynamic and steric effects that act during the growth of supramolecular homoassociates, and take into account the specific binding characteristics of the achiral porphyrin units.

The investigated experimental system consists of diluted solutions of homoassociates of diprotonated meso-sulfonatophenyl substituted porphyrins, which at higher concentrations give colloidlike solutions (*11–13*) that can form lyotropic liquid-crystal structures (*14*). Although all diprotonated compounds of the homologous series of tetraphenyl sulfonate porphyrins ($H_2TPPS_4^{2-}$, $H_2TPPS_3^-$, H_2TPPS_{2a}, and H_2TPPS_{2o}) show very similar trends with respect to the chirality selection phenomenon reported here, the results presented below correspond to the 5,10,15-tris(4-sulfonatophenyl)-20-phenylporphyrin ($H_2TPPS_3^-$).

The specific experimental system was chosen to prove the role of asymmetric forces in the process of chiral selection. First, the aggregation of these diprotonated porphyrins to form mesophaselike supramolecular structures is promoted by concentration as well as by the ionic strength and the acidity of the medium. Second, diluted solutions of these aggregates show circular dichroism (CD) spectra (Fig. 1), without any substantial contribution of linear dichroism (LD) (*15*). Moreover, their optical rotary dispersion (ORD) spectra show curves in agreement with those of the CD spectra (*16*), and the detection of ORD or of CD at the absorption bands is the unambiguous signature of chirality at molecular level (*17*). Finally, a clear relation was detected between the progress of the aggregation (followed by ultraviolet (UV)/visual (vis) spectroscopy) and the ellipticity values of the CD spectra, in such a way that a stable stage of aggregation results in stable signals. Because the samples give the same CD spectra after storage for several months, we conclude that racemization does not occur, and this unambiguously points to a symmetry breaking scenario.

To have a robust evidence of chirality selection for stirred solutions, beyond obscure, nonsystematic, and even highly unreproducible hints of such an effect that had previously appeared in the literature [(*11*), and cited references in (*18*)], our strategy was to select the aggregation procedure most likely to be sensitive to chiral macroscopic forces. We thus chose to promote aggregation by gentle rotary evaporation of very diluted solutions of diprotonated porphyrins, i.e., of the monomeric species. In this way, we enhanced the effect of a true chiral force, represented by the vortex motion (*19*), given the slow dynamics of the evaporation-mediated aggregation (*20*).

In representative experiments, the acidified diprotonated porphyrin solutions (500 ml of 0.12 μM $H_2TPPS_3^-$) were rotary evaporated (≈2 hours), either clockwise (CW) or anticlockwise (ACW), up to a reduction of about. 1/20 of the initial volume (see caption of Fig. 2 for experimental details). These experiments were compared with unstirred solutions, where aggregation was promoted by acidification and whose final concentrations, pH, and ionic strength values were the same, within experimental accuracy, as the rotary evaporated samples.

In Fig. 2A (blank unstirred experiments) the statistical distribution does not show any chirality dominance (pure symmetry breaking). Conversely, in Fig. 2B, for rotary evaporated samples, chirality selection is observed that is dependent on the rotation direction of the rotary evaporator (biased sym-

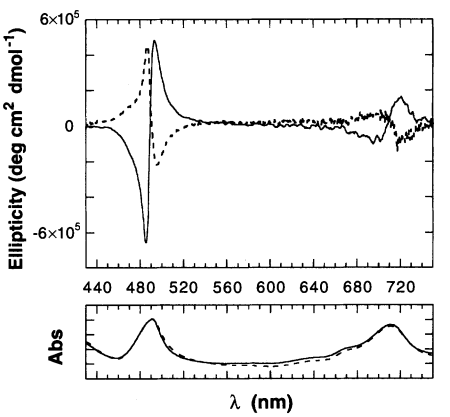

Fig. 1. CD and UV/vis spectra of two solutions (3 μM) of homoassociates of $H_2TPPS_3^-$ corresponding to two characteristic experiments of Fig. 2B (vortex direction during the rotary evaporation; solid lines, CW; dashed lines, ACW). The bisignate CD signals are a consequence of the degenerate character of the transitions. The positive (negative) chirality sign is taken for CD bisignate signals at the absorption wavelength of the Soret(B)-band of the J-aggregate (490 nm) with positive (negative) values at high wavelengths. The CD samples consisted of relatively large volumes (1.5 ml to 3 ml), corresponding to representative volumes of the tested solutions (about 10 to 20% in volume in the case of the optimized experiments of Fig. 2).

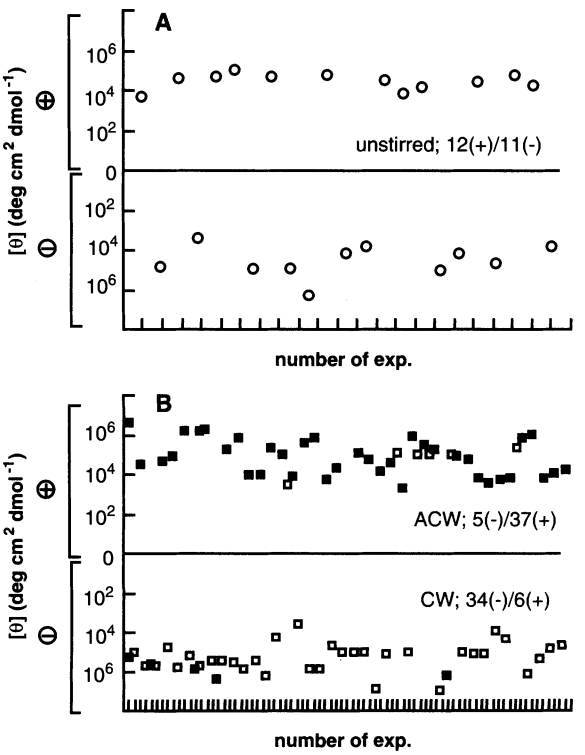

Fig. 2. (**A**) Chirality signs following from the pure symmetry breaking of unstirred solutions: 0.7 g of NaCl (0.6 M) was added to a 20 ml of a 3 μM $Na_3TPPS_3^-$ solution, previously sonicated for 30 min, and after its solubilization the aggregation process was started by the addition of 14 μl of 98% H_2SO_4. (**B**) Chirality signs following the biased symmetry breaking caused by vortex motion: concentration of 500 ml of 0.12 μM solutions of $H_2TPPS_3^-$ (prepared from the trisodium salt, with the addition of 14 μl of H_2SO_4 and 0.5 g of NaCl) was conducted by rotary evaporation (600 ± 50 rpm, inclination of 45°, 55°C, and 25 torr) (blank squares, CW; solid squares, ACW) to 20 ml (i.e., to the same concentrations as for the experiments of Fig. 1); rotary evaporation typically takes about 2 hours. In the case of unstirred solutions (A), the ellipticity values increase with time up to a constant, and CD spectra were typically recorded after 3 hours of aggregation. For stirred solutions (B), the CD spectra were recorded immediately after finishing the experiment, but no substantial changes in ellipticity values were detected after several months.

metry breaking). As shown in Fig. 2B, chirality was coherently induced by stirring with a probability of about 85%.

The structure of these homoassociates at the nanoscale level is schematically represented in Fig. 3. It consists of ribbonlike J-aggregates (side-to-side stepped porphyrins), which aggregate face-to-face, giving rise to an H-like homoassociation (*11, 12, 14*). The J-aggregation occurs through intermolecular electrostatic and hydrogen bonding interactions between the anionic sulfonato groups and the positively charged porphyrin rings. In this way, intermolecularly stabilized zwitterions are formed. It is worth remarking, for what follows, that 180°, 90°, and −90° arrangements (with respect to a simple strand) are indeed possible through peripheral substitution with the sulfonatophenyl groups (Fig. 3). The folding of the preferred long symmetry axis of the J-aggregate constitutes the elementary chiral fluctuation (*3, 4, 21*). CD spectroscopy used here to detect the chirality, is a technique that detects chirality features at the nanoscale level, as represented by the exciton coupled porphyrin chromophore (*22*). In our case, the folding is an extended chiral chromophore (see inset of Fig. 3), which allows one to detect the enantiomeric excess of chiral foldings through chiro-optical methods.

A second step in the interpretation of our results is the proper description of the hydrodynamic effects. The closest previously reported scenario is that of chiral symmetry breaking during crystallization (*4–6, 21*). In this context, stirring is understood to indistinctly select chirality by promoting competitive secondary nucleation that reproduces the initial and randomly adopted chirality of the parent nucleus. In our system, recent mesoscopic analysis of these porphyrin condensates with static and dynamic light scattering techniques (*13, 23, 24*) supports the view of a hierarchical and stable size distribution of these aggregates, at least beyond some advanced stage of the aggregation. Such a hierarchy is particularly simple because it basically consists of relatively small oligomeric blocks being progressively incorporated into massive H-type bundles of J-aggregates (Fig. 3). According to this picture, the relative swirling trajectories of the yet to be incorporated small blocks would nearly reproduce the funnel-like streamlines created by the vortex, before collapsing into the practically motionless large size aggregates. In other words, the motion of the oligomeric blocks relative to the H-supramolecular structures would be diasterotropic once a particular vorticity direction is externally prescribed. Finally, such a preferential asymmetric accretion would be imprinted into the aggregated material as the newly arriving blocks weld at definite arrangements, mediated by short-range interactions that are involved, as mentioned above, in the porphyrin aggregation (see inset of Fig. 3). Another crucial ingredient is still needed to preserve and actually enhance a particular handedness for each vorticity sign, while largely unfavoring the opposite virtual enantiomers (*25*), which is the autocatalytic effect mediated in our case by a steric hindrance acting on the successive oligomers as they are incorporated into the H-bundle. Such an autocatalysis would coherently propagate the "elementary" chiral fluctuations into the growing supramolecular aggregate.

We now put our results into the perspective of symmetry breaking bifurcations. The picture we should retain of the process at hand is that it corresponds to an imperfect (biased) bifurcation mediated by an asymmetric force. Such a scenario had long been predicted theoretically (*2, 3*) as a result of the extreme sensitivity of symmetry breaking realizations to even small asymmetric forces. This is singularly important when the bifurcation point is slowly crossed as the control parameter is gently varied. Such a condition in our case is achieved by the slow progress of the condensation process.

From the perspective of the above results, one could look toward designing experiments aimed at preparing chiral soft materials that would be further used for symmetry amplification (*26, 27*) at lower scale levels, i.e., as chiral catalysts for chemical synthesis and chiral selective membranes. On the other hand, colloids, micelles, and lyotropic liquid crystals are presently well recognized for their preponderant role at many levels of cellular structures (*28*). One is thus tempted to speculate about the role of the different hemispherical vorticity in relation to the origin of biological chirality (*29*). In this regard, symmetry breaking of mesophases and chiral microobjects, whose chirality could have been induced by the permanent sign of vortices in primeval mixtures, could have acted as initial asymmetric factors at prebiotic stages (*30*).

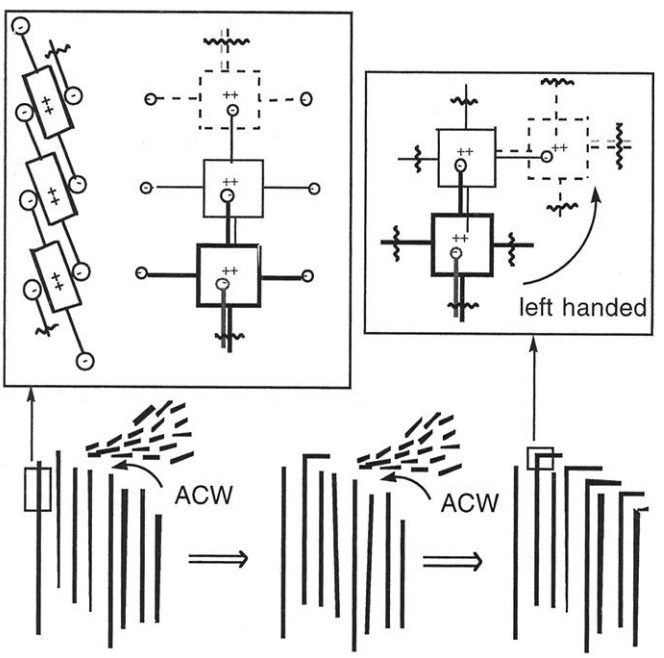

Fig. 3. Two-dimensional schematic picture of the autocatalytic process leading to chiral selection in the supramolecular association of the substituted porphyrins. Diasterotropic relative motion of oligomeric blocks and steric hindrance effects on the folding of the J-chains by aggregation would explain sign induction by vortical stirring. Insets show the three-dimensional extended chromophores in J-aggregates of diprotonated porphyrins. According to the exciton coupling model for π systems (*22*) a right-handed (left-handed; i.e., the case shown in the inset of Fig. 3) chirality results in a +(−) chirality sign. Then ACW (CW) vortex would generate a left-handed (right-handed) chirality.

References and Notes

1. G. Helmchen, R. W. Hoffmann, J. Mulzer, E. Schauman, Eds., *Stereoselective Synthesis*, vols. 1 to 10 of *Houben-Weyl Methods of Organic Chemistry* (Thieme, Stuttgart, Germany, 1996).
2. D. K. Kondepudi, I. Prigogine, *Modern Thermodynamics* (Wiley, New York, 1998), pp. 436–438.
3. D. K. Kondepudi, G. W. Nelson, *Physica A* **125**, 465 (1984).
4. J. Jacques, A. Collet, S. H. Wilen, *Enantiomers, Racemates, Resolutions* (Wiley, New York, 1981).
5. D. K. Kondepudi, R. J. Kaufman, N. Singh, *Science* **250**, 975 (1990).
6. D. K. Kondepudi, K. L. Bullock, J. A. Digits, J. K. Hall, J. M. Miller, *J. Am. Chem. Soc.* **115**, 10211 (1993).
7. D. K. Kondepudi, J. Laudadio, K. Asakura, *J. Am. Chem. Soc.* **121**, 1448 (1999).
8. X. Qiu, J. Ruiz-Garcia, K. J. Stine, C. M. Knobler, J. V. Selinger, *Phys. Rev. Lett.* **67**, 703 (1991).
9. D. K. Schwartz, R. Viswanathan, J. A. N. Zasadzinski, *Phys. Rev. Lett.* **70**, 1267 (1993).
10. H. V. Berlepsch, C. Böttcher, A. Quart, S. Dähne, S. Kirstein, *J. Phys. Chem. B* **104**, 5255 (2000).
11. O. Ohno, Y. Kaizu, H. Kobayashi, *J. Chem. Phys.* **99**, 4128 (1993).
12. R. Rubires *et al.*, *New J. Chem.* **23**, 189 (1999).
13. N. Micali, F. Mallamace, A. Romeo, R. Purrello, L. Monsu Scolaro, *J. Phys. Chem. B* **104**, 5897 (2000).
14. J. M. Ribó *et al.*, *Mater. Sci. Eng. C* **11**, 107 (2000).
15. We were singularly concerned with excluding LD contributions in the experimental CD spectra reported in Fig. 2. In this respect, we checked that CD

spectra did not change either when they were recorded rotating the cuvette 90° around the light axis or after strong cuvette shaking. Moreover, rectangular cuvettes of 0.5 cm and a 1-cm optical path were used, which exclude the alignments of mesophases that thin cuvettes can cause. In this sense, the chirality previously detected in cyanine dye J-aggregates was later rejected on the basis of LD artifacts [see cited references in (*18*)]. However, recent reports [e.g., (*10*)] on similar J-aggregates have excluded LD contributions with similar experimental cautions to those reported here. We detected dichroic signals due to these artifacts in the case of solutions containing very large aggregates, but these solutions were obtained under different experimental conditions. Finally, we found that because of resonance light scattering effects at the absorption bands of these homoassociates (*31*), differential scattering may be an important contribution to the CD spectra (*32*), but such contributions are also related to the molecular chirality (*33*).

16. This was observed for the ORD spectra recorded in a Pockel's cell instrument as well as for those obtained in a calcite prisms instrument.
17. Two important questions are worth remarking on at this point: (i) the UV/vis absorption bands of the homoassociates occur at very different wavelengths than those of the monomeric species (*11–13*), allowing us to attribute unambiguously the detected chirality to the homoassociate chromophores; (ii) the huge absorptivity of the porphyrin chromophor transitions results in high rotational strengths and leads to high sensitivities in the detection of enantiomeric excesses.
18. M. Avalos *et al.*, *Chem. Rev.* **98**, 2391 (1998).
19. True chirality meets the nonexchange condition between enantiomers through the space reversal as well as with the time reversal operators (e.g., a vortex translation). False chirality meets this condition through the space reversal operator (e.g., rotation in a gravitational field) [(*18*); L. D. Barron, *Chem. Soc. Rev.* **15**, 189 (1986)].
20. In fact, complementary experiments conducted with magnetically stirred solutions where aggregation was suddenly fostered by acidification of a free base porphyrin solution, at near to constant ionic strength, did not show any substantial signature of chiral selection.
21. G. Bersuker, *J. Chem. Phys.* **110**, 10907 (1999).
22. N. Harada, K. Nakanishi, *Circular Dichroism Spectroscopy. Exciton Coupling in Organic Spectroscopy* (University Science Books, Mill Valley, CA, 1983).
23. P. J. Collings *et al.*, *J. Phys. Chem. B* **103**, 8474 (1999).
24. K. Misawa, T. Kobayashi, *J. Chem. Phys.* **110**, 5844 (1999).
25. O. Katzenelson, H. Z. Hel-Or, D. Avnir, *Chem. Eur. J.* **2**, 174 (1996).
26. B. L. Feringa, R. A. van Delden, *Angew. Chem. Int. Ed.* **38**, 3419 (1999).
27. C. Girard, H. B. Kagan, *Angew. Chem. Int. Ed.* **37**, 2922 (1998).
28. J. M. Seddon, R. H. Templer, in *Handbook of Biological Physics*, R. Lipowsky *et al.*, Eds. (Elsevier Science, New York, 1995), vol. 1, pp. 97–160.
29. S. F. Mason, *Nature* **311**, 19 (1984).
30. V. Avetisov, V. Goldanskii, *Proc. Natl. Acad. Sci. U.S.A.* **93**, 11435 (1996).
31. R. F. Pasternack, P. J. Collings, *Science* **269**, 935 (1995).
32. R. Rubires, J.-A. Farrera, J. M. Ribó, *Chem. Eur. J.* **7**, 436 (2001).
33. C. Bustamante, I. Tinoco Jr., M. F. Maestre, *Proc. Natl. Acad. Sci. U.S.A.* **80**, 3568 (1983).
34. Supported by DGI (Spanish Government) and CUR (Generalitat de Catalunya).

19 March 2001; accepted 19 April 2001

Modulation of Cell Proliferation by Heterotrimeric G Protein in *Arabidopsis*

Hemayet Ullah,[1] Jin-Gui Chen,[1] Jeff C. Young,[2]* Kyung-Hoan Im,[1] Michael R. Sussman,[2] Alan M. Jones[1]†

The α subunit of a prototypical heterotrimeric GTP-binding protein (G protein), which is encoded by a single gene (*GPA1*) in *Arabidopsis*, is a modulator of plant cell proliferation. *gpa1* null mutants have reduced cell division in aerial tissues throughout development. Inducible overexpression of *GPA1* in *Arabidopsis* confers inducible ectopic cell division. *GPA1* overexpression in synchronized BY-2 cells causes premature advance of the nuclear cycle and the premature appearance of a division wall. Results from loss of function and ectopic expression and activation of *GPA1* indicate that this subunit is a positive modulator of cell division in plants.

Heterotrimeric G proteins regulate cell growth, differentiation, and transformation in animal cells (*1*). Many growth factors activate receptors that transmit signals to the cytoplasm through heterotrimeric G proteins. Of the 17 Gα subunits that have been cloned, 10 couple mitogenic signaling (*2*, *3*). Studies of the interaction between Gα subunits and proliferation support the emerging view that the α subunits form a new class of oncogenes (*4–6*).

[1]Department of Biology, University of North Carolina at Chapel Hill, Chapel Hill, NC 27599, USA. [2]Cell and Molecular Biology Program and the Department of Horticulture, University of Wisconsin, 1575 Linden Drive, Madison, WI 53706, USA.

*Present address: Biology Department, MS-9160, Western Washington University, Bellingham, WA 98225, USA.

†To whom correspondence should be addressed at Department of Biology, CB#3280, University of North Carolina at Chapel Hill, Chapel Hill, NC 27599–3280, USA. E-mail: alan_jones@unc.edu

The *Arabidopsis* genome contains a single prototypical Gα (*GPA1*) gene, offering a unique advantage over its animal counterparts to dissect its role in cell proliferation. Various signals such as auxin, cytokinin, brassinosteroids, light, sucrose, stress, and developmental factors modulate cell proliferation in plants as well (*7*). On the basis of *GPA1* expression in actively dividing cells, it has been suggested that GPA1 is involved in promoting active cell division (*8*), a notion supported by the observation that a rice Gα mutant confers a dwarf phenotype (*9*).

By screening an *Arabidopsis* transferred DNA (T-DNA) insertion population (*10*), two recessive mutant alleles, *gpa1-1* and *gpa1-2*, were identified and shown by direct sequencing to harbor T-DNA in the predicted seventh intron (*gpa1-1*) and in the eighth exon (*gpa1-2*) (Fig. 1A). Northern hybridization results showed the expected size of truncated mutant transcripts (Fig. 1C) and that the steady-state levels of the mutant transcripts were not affected in the dark. The insertion eliminates four of its five polypeptide loops required for GTP binding (*11*), the guanosine triphosphatase (GTPase) domain, and the effector loop. On the basis of parallel structure-function studies on animal Gα, the *Arabidopsis* GPA1 mutant proteins are predicted to be nonfunctioning. Western hybridization with antiserum directed against a recombinant *Arabidopsis* GPA1 showed that, in the mutant lines, no Gα protein of any size was detected. This indicates that the T-DNA insertions in both *gpa1-1* and *gpa1-2* produce null alleles or that the truncated gene product is no longer recognizable by the antibodies to GPA1 (Fig. 1D).

gpa1 mutants displayed phenotypes that were consistent with a reduction in cell division throughout development, although with contrasting effects on organ morphogenesis. In light-grown seedlings, *gpa1* leaf size and morphology were maintained despite fewer cells composing this organ. Compensation by increased cell size for reduced cell number during organ morphogenesis has been documented frequently (*12–14*), supporting the theory that the individual cell is not always the basic unit of morphogenesis in plants. However, *gpa1* mutants also illustrate that a reduction of cell number results in reduced hypocotyl length, providing the alternative example of morphogenesis.

Exposure of wild-type plants to light marks the start of photomorphogenic development called de-etiolation. Both *gpa1* mutant alleles displayed partial de-etiolation (Fig. 2). Dark-grown *gpa1* mutant seedlings had short hypocotyls and open hooks typical of light-irradiated seedlings, but the root and cotyledon phenotypes were dark-grown wild type (WT). Scanning electron microscopy revealed that the constitutive hook opening is due to the normal expansion of adaxial cells